Nonlinear Magnetic Circuit Analysis for a Novel Stator Doubly Fed Doubly Salient Machine

K. T. Chau, *Member, IEEE*, Ming Cheng, *Senior Member, IEEE*, and C. C. Chan, *Fellow, IEEE*

***Abstract*—A novel stator doubly fed doubly salient (SDFDS) machine is proposed, and a nonlinear magnetic circuit (NMC) model is developed for the analysis of the SDFDS machine. Based on the NMC model, the static characteristics of an 8/6-pole SDFDS machine are analyzed using specific permeance calculations, in which the interaction between field and armature currents as well as the magnetic saturation are taken into account. The proposed NMC modeling is verified using both finite-element analysis and experimentation.**

***Index Terms*—Analytical model, doubly salient machine, magnetic circuits, permeance calculation, static characteristics.**

I. Introduction

With ever increasing concerns on the environment, the development of electric vehicles (EVs) has taken on an accelerated pace. To enable EVs to directly compete with gasoline vehicles, the EV motor aims to pursue high efficiency, high power density, high controllability, wide speed range, and maintenance-free operation [1]. In order to pursue these goals, the doubly salient permanent-magnet (DSPM) machine has been proposed which incorporates both the advantages of both PM brushless and switched reluctance (SR) machines [2], [3]. However, it still suffers from drawbacks of high PM material cost and uncontrollable PM flux. Also, the use of finite-element analysis (FEA) for its design optimization is very time-consuming when different geometric dimensions need to be considered [4].

In this paper, a novel machine topology, namely, the stator doubly fed doubly salient (SDFDS) machine is first proposed, which not only solves the fundamental problems of the DSPM machine, but also offers the flexibility to optimize the efficiency on-line. Following the spirit of the magnetic circuit approach for the DSPM machine [4], the nonlinear magnetic circuit (NMC) modeling method is developed for the SDFDS machine, which functions to effectively analyze and efficiently optimize the proposed machine.

II. Design

Fig. 1 shows the structure of an 8/6-pole (eight stator poles and six rotor poles) SDFDS machine. It consists of two types of stator windings: a polyphase armature winding and a dc field winding. Since the dc current in the field winding is independently controllable, this machine can readily control the field flux for flux weakening operation and optimize efficiency on-line. Notice that flux weakening operation is necessary for high-speed EV cruising, whereas efficiency optimizing control is essential for long EV driving range.

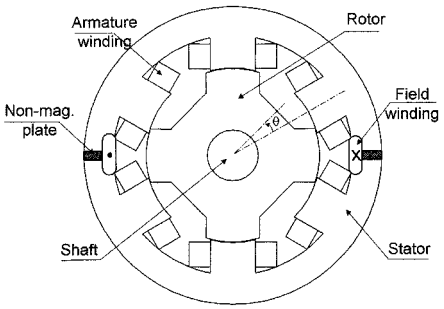

Fig. 1. Proposed SDFDS machine structure.

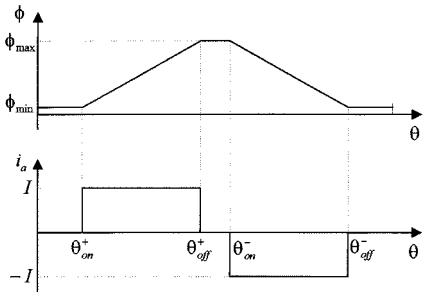

Fig. 2. Operating waveforms.

Fig. 2 shows the operating waveforms of field flux ϕ and armature current i_a versus rotor position θ. When a rotor pole is entering the zone occupied by a conductive phase, the flux is increasing. If a positive current is applied to the phase winding, a positive torque will be produced. When the rotor pole is leaving the stator pole from the aligned position, the flux is decreasing. A positive torque is also produced if a negative current is applied to the winding. Thus, two possible torque producing zones are fully utilized.

III. Modeling

Fig. 3 shows the proposed NMC model of the 8/6-pole SDFDS machine at the minimum flux position $(\theta = 0°)$ of the phase A, where θ is defined as the angle between the stator pole central line and the rotor slot central line as shown in Fig. 1. In the model, p_{PS}, $p_{YS}(p'_{YS})$, p_{PR}, and p_{YR} are the pole and yoke permeances of the stator and rotor, respectively, which vary with the nonlinear saturation in the corresponding magnetic paths, whereas p_{PYL}, p_{PL}, p_F, p_{FL}, and p_A are

Manuscript received February 5, 2002; May 28, 2002. This work was supported by the Hong Kong Research Grants Council under Project HKU 7035/01E.

K. T. Chau and C. C. Chan are with the Department of Electrical and Electronic Engineering, The University of Hong Kong, Pokfulam, Hong Kong (e-mail: ktchau@eee.hku.hk; ccchan@eee.hku.hk).

M. Cheng is with the Department of Electrical Engineering, Southeast University, Nanjing 210096, China (e-mail: mcheng@seu.edu.cn).

Digital Object Identifier 10.1109/TMAG.2002.803582.

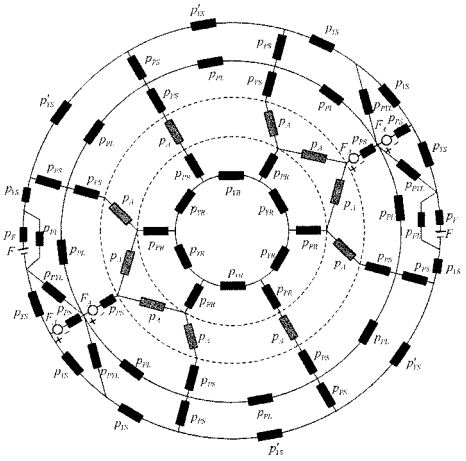

Fig. 3. Proposed NMC model.

the permeances of stator pole-to-yoke leakage flux, stator pole-to-pole leakage flux, nonmagnetic plate flux, field leakage flux, and air-gap flux, respectively, which are of constant permeability. The field magnetizing force is represented by an equivalent magnetomotive force (MMF) F. In order to take into account the leakage flux from the stator pole of the conducting phase (phase A) to the stator yoke, the armature MMF supplied by the phase A winding, the stator pole permeance, and the stator yoke permeance are represented by two F_A, two p_{PS}, and two p_{YS}, respectively, and then p_{PYL} is connected between the middle points of two p_{PS} and two p_{YS}, as shown in Fig. 3. When there is no need to consider this leakage flux, p'_{YS} stands for the stator yoke permeance.

IV. Analysis

According to the position of the rotor with respect to the stator, there are eight possible regions as defined by Region 1 $0 \le \alpha < \alpha_1$, Region 2 $\alpha_1 \le \alpha < \alpha_2, \ldots$, and Region 8 $\alpha_7 \le \alpha < \alpha_8$, where α is the angle between the central lines of stator and rotor poles, and $\alpha_1 = 1/2\,(\beta_r - \beta_s)$, $\alpha_2 = 1/2(\tau_s - \beta_r)$, $\alpha_3 = 1/2(\tau_r - \tau_s)$, $\alpha_4 = 1/2(\beta_s + \beta_r)$, $\alpha_5 = 1/2(\tau_r - \beta_s)$, $\alpha_6 = 1/2(\tau_s + \beta_r)$, $\alpha_7 = 1/2(\tau_r + \beta_s)$, $\alpha_8 = 1/2(\tau_s + \tau_r)$, in which τ_s is the stator pole pitch, τ_r the rotor pole pitch, β_s the stator pole arc, and β_r the rotor pole arc. Fig. 4 illustrates the rotor positions corresponding to Region 1 and $\alpha = \alpha_1$, respectively. Also, each region is divided into several sections, in which the magnetic parameters within each section are considered to be constant. For example, Region 1 is divided into five sections that can be expressed as $a = [1/2(\tau_s - \beta_r) + \alpha]r_{\mathrm{si}}$, $b = (\alpha_1 - \alpha)r_{\mathrm{si}}$, $c = \beta_s r_{\mathrm{si}}$, $d = (\alpha_1 + \alpha)r_{\mathrm{si}}$, and $e = 1/2(\tau_s - \beta_s)r_{\mathrm{si}} - d$, where r_{si} is the stator inner radius. Moreover, in order to analytically describe the flux lines by semicircular and straight segments, the edges of the stator pole as well as the left and right edges of the rotor pole are inclined by the angles of β_1, β_2, and β_3, respectively. As a rule of thumb, these angles can be represented by empirical formulas [5]. Corresponding to β_1, β_2, and β_3, the interconnection points between semicircular and straight segments are given by x_1, x_2, and x_3.

The air-gap specific permeance p_A of a flux tube can readily be calculated by

$$p = \frac{\mu_0 A_m}{l_m} \tag{1}$$

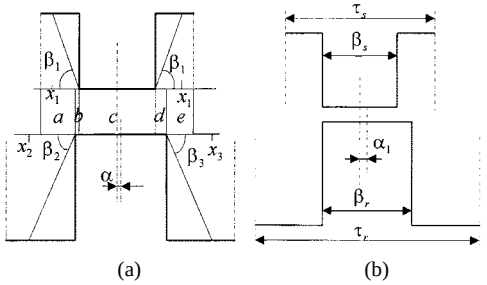

(a) (b)

Fig. 4. Rotor positions. (a) Region 1. (b) $\alpha = \alpha_1$.

where A_m is the width of the flux tube, l_m is the length of flux path between equipotential surfaces, and μ_0 is the permeability of free space. In the following, Region 1 is used to illustrate the formulation of the air-gap specific permeance. By using (1), the p_A in Section a is given by

$$\begin{aligned} p_{Aa} &= \int_0^a \frac{\mu_0 dx}{g_0 + \beta_1(x+b) + \beta_2 x} \\ &= \frac{\mu_0}{\beta_1 + \beta_2} \ln\left[1 + \frac{(\beta_1 + \beta_2)a}{g_0 + \beta_1 b}\right] \end{aligned} \tag{2}$$

where g_0 is the air-gap length, provided that $x_2 \ge a$. Otherwise, it should be expressed as

$$\begin{aligned} p_{Aa} = {} & \frac{\mu_0}{\beta_1 + \beta_2} \ln\left[1 + \frac{(\beta_1 + \beta_2)x_2}{g_0 + \beta_1 b}\right] \\ & + \frac{\mu_0}{\beta_1} \ln\left[1 + \frac{\beta_1(a - x_2)}{g_0 + h_r + \beta_1(x_2 + b)}\right]. \end{aligned} \tag{3}$$

In Section b, it is given by

$$p_{Ab} = \int_0^b \frac{\mu_0 dx}{g_0 + \beta_1 x} = \frac{\mu_0}{\beta_1} \ln\left[1 + \frac{\beta_1 b}{g_0}\right]. \tag{4}$$

In Section c, it is simply written as

$$p_{Ac} = \frac{\mu_0 c}{g_0}. \tag{5}$$

Similar to (4), in Section d, it is given by

$$p_{Ad} = \int_0^d \frac{\mu_0 dx}{g_0 + \beta_1 x} = \frac{\mu_0}{\beta_1} \ln\left[1 + \frac{\beta_1 d}{g_0}\right]. \tag{6}$$

Similar to (2), in Section e, it is given by

$$\begin{aligned} p_{Ae} &= \int_0^e \frac{\mu_0 dx}{g_0 + \beta_1(x+d) + \beta_3 x} \\ &= \frac{\mu_0}{\beta_1 + \beta_3} \ln\left[1 + \frac{(\beta_1 + \beta_3)e}{g_0 + \beta_1 d}\right] \end{aligned} \tag{7}$$

provided that $x_3 \ge e$. Otherwise, it is given by

$$\begin{aligned} p_{Ae} = {} & \frac{\mu_0}{\beta_1 + \beta_3} \ln\left[1 + \frac{(\beta_1 + \beta_3)x_3}{g_0 + \beta_1 d}\right] \\ & + \frac{\mu_0}{\beta_1} \ln\left[1 + \frac{\beta_1(e - x_3)}{g_0 + h_r + \beta_1(d + x_3)}\right]. \end{aligned} \tag{8}$$

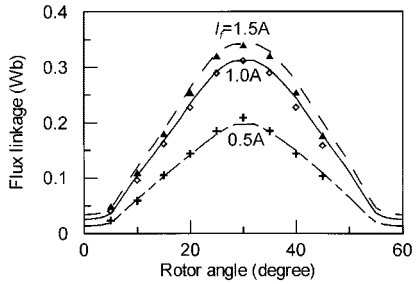

Fig. 5. Calculated flux linkage characteristics.

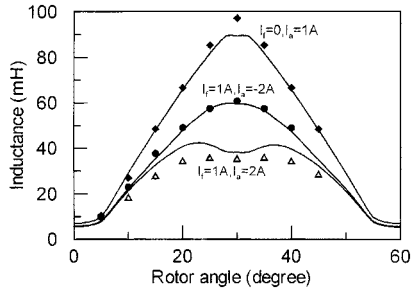

Fig. 6. Calculated inductance characteristics.

Therefore, making use of (2)–(8), the total air-gap specific permeance in Region 1 is formulated as

$$p_A(\alpha) = \sum_{i=a}^{e} p_{Ai}. \tag{9}$$

For other regions, the total air-gap specific permeances can be derived in a similar way. The corresponding formulas are omitted for the sake of conciseness. On the other hand, the specific permeance of iron in the magnetic circuit can also be determined using (1), but with a nonconstant permeability μ that needs to be determined by iterative calculation.

Since the number of branches of the NMC model varies with the rotor position while the number of nodes is fixed, nodal analysis is employed. The nodal equation is given by

$$\mathbf{G}(\mu_i)\mathbf{F}_m = \Phi_s(\mu_i) \tag{10}$$

where μ_i is the permeability of branch i, $\mathbf{G}(\mu_i)$ is the node permeance matrix, $\mathbf{F}_m$ is the node magnetic potential vector, and $\Phi_s(\mu_i)$ is the node magnetic flux source vector.

V. Characteristics

By rotating the rotor of the SDFDS machine from 0° to 60° step by step, its static characteristics including the flux linkage, inductance, and back-electromotive force (back-EMF) are readily obtained. Fig. 5 shows the no-load flux linkages (solid and dashed lines) at different field currents calculated by the proposed NMC model. The results by FEA (discretely marked) are also shown in Fig. 5, indicating that there is a good agreement between them.

From the flux linkage characteristics, the inductance can be easily deduced. Fig. 6 shows the inductance characteristics at different field currents and armature currents. As expected, the unsaturated inductance ($I_f = 0$) agrees with the FEA results (discretely marked). Moreover, because of magnetic saturation, the calculated inductances under $I_f = 1$ A are significantly lower than the unsaturated one. It can also be seen that when the armature current acts to strengthen the field flux, magnetic saturation becomes more serious, resulting in lower inductance.

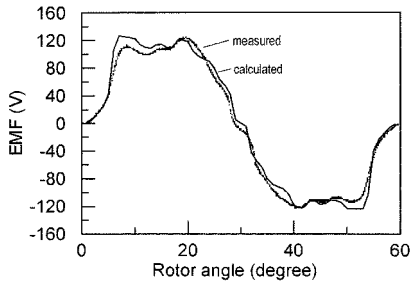

Fig. 7. Calculated and measured back-EMF characteristics.

Similarly, the back-EMF can be directly deduced from the flux linkage. At the rated speed of 1500 rpm and $I_f = 1$ A, the calculated back-EMF characteristic is shown in Fig. 7. After prototyping the machine, this back EMF is measured under the same conditions and also given in Fig. 7.

It may be seen from Figs. 6 and 7 that there are some discrepancies between the results obtained from the NMC model and the FEA or experiments. The reasons are due to two factors: one is the local saturation in pole tips, which is difficult to be taken into account accurately in the NMC model; another is the imperfect manufacture of the prototype machine. Nevertheless, these discrepancies are reasonable and expected because the proposed NMC approach takes the advantage of analytical modeling to rapidly determine the static characteristics of SDFDS machines with different dimensions and excitation conditions. The degradation of accuracy is tolerable in view of the time saving. Further efforts are being attempted to model the local saturation in pole tips more accurately.

VI. Conclusion

In this paper, a novel SDFDS machine and its NMC modeling method have been presented. Based on this NMC model, the static characteristics of an 8/6-pole SDFDS machine have been analyzed using specific permeance calculations, in which the interaction between field and armature currents as well as the magnetic saturation are taken into account. The proposed NMC modeling method has been verified by using both FEA and experimental measurement. It offers the advantage to effectively and efficiently determine the static characteristics of SDFDS machines under different dimensions and excitation conditions with reasonable accuracy.

References

[1] C. C. Chan and K. T. Chau, *Modern Electric Vehicle Technology*. Oxford, U.K.: Oxford Univ. Press, 2001, pp. 67–83.

[2] Y. Liao, F. Liang, and T. A. Lipo, "A novel permanent magnet motor with doubly salient structure," *IEEE Trans. Ind. Applicat.*, vol. 31, pp. 1069–1078, Sept./Oct. 1995.

[3] M. Cheng, K. T. Chau, and C. C. Chan, "Design and analysis of a new doubly salient permanent magnet motor," *IEEE Trans. Magn.*, vol. 37, pp. 3012–3020, July 2001.

[4] M. Cheng, K. T. Chau, C. C. Chan, E. Zhou, and X. L. Huang, "Nonlinear varying-network magnetic circuit analysis for doubly salient permanent magnet motors," *IEEE Trans. Magn.*, vol. 36, pp. 339–348, Jan. 2000.

[5] R. Pohl, "Theory of pulsating-field machines," *J. Inst. Elect. Eng.*, pt. II, vol. 93, pp. 37–47, 1946.